CEAS-GNC-2024-056

EuroGNC Navigation Guidance Control CEAS Bristol, UK June 11th-13th 2024
University of BRISTOL ROYAL AERONAUTICAL SOCIETY AIAA

Adaptive Formation Control of Unmanned Aerial Vehicles in Wind

Toufik Souanef Lecturer, School of Aerospace Transport and Manufacturing, Cranfield University, Cranfield, MK43 0AL, UK. toufik.souanef@cranfield.ac.uk

Huamin Jia Senior Lecturer, School of Aerospace Transport and Manufacturing, Cranfield University, Cranfield, MK43 0AL, UK h.jia@cranfield.ac.uk

James F. Whidborne Professor, School of Aerospace Transport and Manufacturing, Cranfield University, Cranfield, MK43 0AL, UK. j.f.whidborne@cranfield.ac.uk

ABSTRACT

This paper introduces an approach to address the challenge of wind disturbances in the context of fixed-wing UAV formation control. It presents a robust adaptive controller that explicitly accounts for the time-varying nature of wind speed, offering a practical solution for real-world scenarios characterized by parametric uncertainties and external disturbances. By considering the dynamic behavior of wind, including phenomena like wind shear and gusts, the design of the controller becomes more realistic, and its analysis gains rigor, enhancing the system robustness. The effectiveness of the proposed controller is demonstrated by simulations.

Keywords: Formation Control, UAV Control, UAV path-following, Adaptive Control

1 Introduction

Small fixed-wing Unmanned Aerial Vehicles (UAVs) that is, with wingspans less than 2 meters and payload smaller than 2 kg are gaining growing interest because of their low cost, high maneuverability and simple maintenance [1]. These UAVs find application in a broad spectrum of military and civilian missions [2–8]. Employing small UAVs in a formation can yield several advantages, such as reduced task completion times, enhanced overall performance, and the ability to undertake diverse missions in complex or constrained environments. This concept is well-supported by [9], [10], and [11].

Research in mobile robotics has significantly influenced the development of UAV formation control. The leader-follower architecture is as one of the most widely adopted methods for achieving formation control. In this framework, a designated leader, or a virtual leader, follows a predefined trajectory, while the followers maintain desired relative positions with respect to it through the implementation of specific control techniques, as explained by [12]. However, as a special type of robot, fixed-wing UAVs have some particular properties owing to their special dynamics [13] which constrain the problem. Firstly, a fixed-wing UAV is an under-actuated system, and its kinematics on the horizontal plane can be simplified to a unicycle system [14]. Secondly, the aircraft must maintain a positive forward minimum airspeed above the stall speed [15].

Several methods for linear control have been proposed to achieve leader-follower formation control for fixed-wing UAVs. One approach is based on Linear Quadratic (LQ) control, which utilizes linearizsd

equations of motion [16]. Another method involves PID control for UAV formation, with results presented in study [17]. More advanced approaches have also been applied. A design based on feedback linearisation was presented in [18], ensuring global stability for the entire system. Reference [19] introduced an adaptive approach for UAV formation control, addressing unknown leader commands and vortex forces in velocity and heading angle dynamics. Second order sliding mode techniques were seen to achieve perfect UAV formation tracking affected by unknown bounded disturbances in [20]. The research of [21] proposed a fuzzy controller for achieving three-dimensional formation control of fixed-wing UAVs with unknown nonlinear dynamics. Reference [22] developed a seeker-based formation control formulation that eliminates the necessity of communication networks by applying an integral sliding mode controller to account for uncertainties in follower speeds measurements. For addressing dynamic uncertainty and unknown external disturbances in UAV formation, a Model Reference Adaptive Control scheme was developed by [23]. More details can be found in the recent literature reviews on UAV formation control [24, 25] and in references therein.

A significant limitation of small fixed-wing UAVs lies in their extreme sensitivity to wind due to their relatively low speeds. In practice, wind speeds often range from 20% to 60% of the desired airspeed for these UAVs [26]. If a formation controller does not account for wind, it can reduce the trajectory-tracking capabilities of the follower UAVs. Moreover, in scenarios where the wind speed can rapidly change, the UAVs may need to operate at considerable distances from one another, making it crucial for the formulation of the formation control problem to consider varying wind speeds affecting each UAV individually. Another challenge arises from the difficulty of maintaining a constant airspeed for small UAVs, especially in the presence of wind. Consequently, there is a need to develop formation control methods explicitly designed to withstand wind disturbances. However, the previously described approaches often neglect the explicit consideration of wind impact on UAV formation control. The only known approach that addresses formation control of fixed-wing UAVs in windy conditions is presented in [27]. This solution is based on vector field guidance [26]. The main drawback of this method is its assumption of constant wind speed, which does not align with real-world conditions where wind velocities are variable and can change rapidly [28].

A solution to this challenge can be provided through the use of $\mathcal{L}_1$ adaptive control [29]. The benefit of $\mathcal{L}_1$ adaptive control is its capacity for fast and robust adaptation that leads to desired transient performance for both system signals, input and output. These characteristics make it suitable for systems subject to external time-varying disturbances, such as small UAVs motion in wind. The $\mathcal{L}_1$ adaptive control has been applied for various autonomous flight control systems of fixed-wing UAVs [28, 30–36], to cite a few.

The main concept of this work is formulating formation control for fixed-wing UAVs as a control design for systems with parametric uncertainties and external disturbances. The proposed solution is built upon the Multi-Input, Multi-Output (MIMO) $\mathcal{L}_1$ adaptive controller, specifically designed for disturbances with unknown bounds [37]. While the $\mathcal{L}_1$ adaptive control has found application in cooperative and formation control of multiple UAVs [38] and [39], it is important to note that both of these prior approaches did not address the issue of wind. In contrast, the approach proposed in this research explicitly tackles the challenge of fixed-wing UAV formation control in the presence of wind, effectively relaxing the assumption that wind speed remains constant.

The rest of this article is organized as follows. Section II describes the formulation of the problem of UAV formation control. Section III presents the $\mathcal{L}_1$ adaptive formation control. Section IV presents the simulation results. Finally, Section V presents conclusions.

2 Problem Formulation

In practice, the two most commonly used paths for UAVs are straight-lines and circular paths [40]. Both types of paths are usually defined on the horizontal plane with constant altitude and speed. Under these assumptions, the UAV kinematics can be written as follows

$$\begin{pmatrix} \dot{X} \\ \dot{Y} \\ \dot{\psi} \end{pmatrix} = \begin{pmatrix} V_a \cos\psi + W_x \\ V_a \sin\psi + W_y \\ w \end{pmatrix}, \tag{1}$$

where X and Y are respectively the North and East positions of the UAV, V_a is the airspeed, ψ is the heading angle relative to the north, w is the heading rate, and W_x and W_y are wind speeds in the inertial frame.

This model is derived under the assumption that the UAV is in steady level flight. In this case, the airspeed vector is aligned with the x-direction of the body frame, which means that the sideslip angle β is zero.

Assuming a bank to turn strategy, the heading rate of the UAV can be expressed as

$$w = \frac{g}{V_a} \tan\phi, \tag{2}$$

where ϕ is the roll angle and g is the gravity acceleration.

If we consider a leader-follower UAV formation, the leader is denoted l and each follower is denoted i, then the kinematic model of the leader UAV can be written from Fig. 1 as

$$\begin{pmatrix} \dot{X}^l \\ \dot{Y}^l \\ \dot{\psi}^l \end{pmatrix} = \begin{pmatrix} V_a^l \cos\psi_l + W_x^l \\ V_a^l \sin\psi_l + W_y^l \\ w^l = \frac{g}{V_a^l} \tan\phi^l \end{pmatrix}, \tag{3}$$

and the kinematics of the ith follower, for $i = 1 \ldots N$, are given by

$$\begin{pmatrix} \dot{X}^i \\ \dot{Y}^i \\ \dot{\psi}^i \end{pmatrix} = \begin{pmatrix} V_a^i \cos\psi_i + W_x^i \\ V_a^i \sin\psi_i + W_y^i \\ w^i = \frac{g}{V_a^i} \tan\phi^i \end{pmatrix}. \tag{4}$$

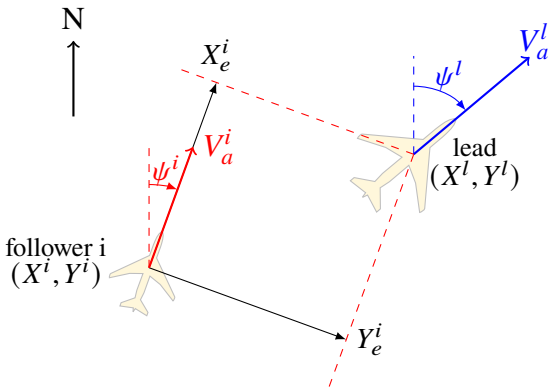

Fig. 1 Leader-Follower formation

The objective is to compute the commanded airspeeds V_a^i and roll angles ϕ^i of the followers that maintain them on the desired paths, despite the presence of wind.The following assumptions are made.

Assumption 1. Each UAV is equipped with a low-level controller that is robust external disturbances.

Assumption 2. The dynamics of the roll are much faster than the heading, hence the inner-loop dynamics can be ignored.

Assumption 3. The leader UAV is equipped with a path-following controller that is robust against wind.

Assumption 4. The state of each UAV is measurable.

Assumption 5. The leader can communicate with the follower UAVs.

Remark 1. In this paper the time dependence is omitted except if it is not clear from the context.

Remark 2. At this point it is important to note that the UAVs might operate at relatively far distances. Furthermore, wind speed can change very quickly. Consequently, it is more realistic to assume that values of wind speed acting on each UAV are different.

The position error of each follower UAV relative to the leader in the global frame can be defined by

$$\begin{pmatrix} P_x^i \\ P_y^i \\ P_\psi^i \end{pmatrix} = \begin{pmatrix} X^l - X^i + X_d^i \\ Y^l - Y^i + Y_d^i \\ \psi^l - \psi^i \end{pmatrix}, \tag{5}$$

where (X_d^i, Y_d^i) are the desired positions of each follower UAV relative to the leader. The previous error can be expressed in the local coordinate frame by

$$\begin{pmatrix} X_e^i \\ Y_e^i \\ \psi_e^i \end{pmatrix} = \begin{pmatrix} \cos\psi^i & \sin\psi^i & 0 \\ -\sin\psi^i & \cos\psi^i & 0 \\ 0 & 0 & 1 \end{pmatrix} \begin{pmatrix} P_x^i \\ P_y^i \\ P_\psi^i \end{pmatrix}. \tag{6}$$

Assuming that X_i^d and Y_i^d are constant, the dynamics of the position error can be written as follows

$$\begin{pmatrix} \dot{X}_e^i \\ \dot{Y}_e^i \\ \dot{\psi}_e^i \end{pmatrix} = \begin{pmatrix} w^i Y_e^i - V_a^i + V_a^l \cos\psi_e^i \\ -w^i X_e^i + V_a^l \sin\psi_e^i \\ -\frac{g}{V_a^i} \tan\phi^i, \end{pmatrix} + d^i, \tag{7}$$

with

$$d^i = \begin{pmatrix} (W_x^l - W_x^i)\cos\psi^i + (W_y^l - W_y^i)\sin\psi^i \\ -(W_x^l - W_x^i)\sin\psi^i + (W_y^l - W_y^i)\cos\psi^i \\ \frac{g}{V_a^l}\tan\phi^l \end{pmatrix}. \tag{8}$$

Considering $x^i = \begin{pmatrix} X_e^i, Y_e^i, \psi_e^i \end{pmatrix}^\top$ and $u^i = \begin{pmatrix} V_a^i, \phi^i \end{pmatrix}^\top$, the system can be written as

$$\begin{pmatrix} \dot{x}_1^i \\ \dot{x}_2^i \\ \dot{x}_3^i \end{pmatrix} = \begin{pmatrix} w^l x_2^i - u_1^i + V_a^l \cos x_3^i \\ -w^l x_1^i + V_a^l \sin x_3^i \\ -\frac{g}{V_a^i}\tan u_2^i \end{pmatrix} + d_i. \tag{9}$$

The system in (9) is a standard formulation of a nonlinear control system in the presence of external time-varying disturbances defined by

$$\begin{aligned} \dot{x}^i &= f(x^i, u^i) + d^i(t) \\ y^i &= Cx^i. \end{aligned} \tag{10}$$

tHE controlled outputs are the positioning errors X_e^i and Y_e^i. Hence

$$C = \begin{pmatrix} 1 & 0 & 0 \\ 0 & 1 & 0 \end{pmatrix}.$$

The objective is to compute the control commands u^i, for each follower UAV, that stabilize the system and maintain the followers on the desired paths, despite the presence of wind. The proposed method is based on $\mathcal{L}_1$ adaptive control. The proposed architecture is shown in Fig. 2.

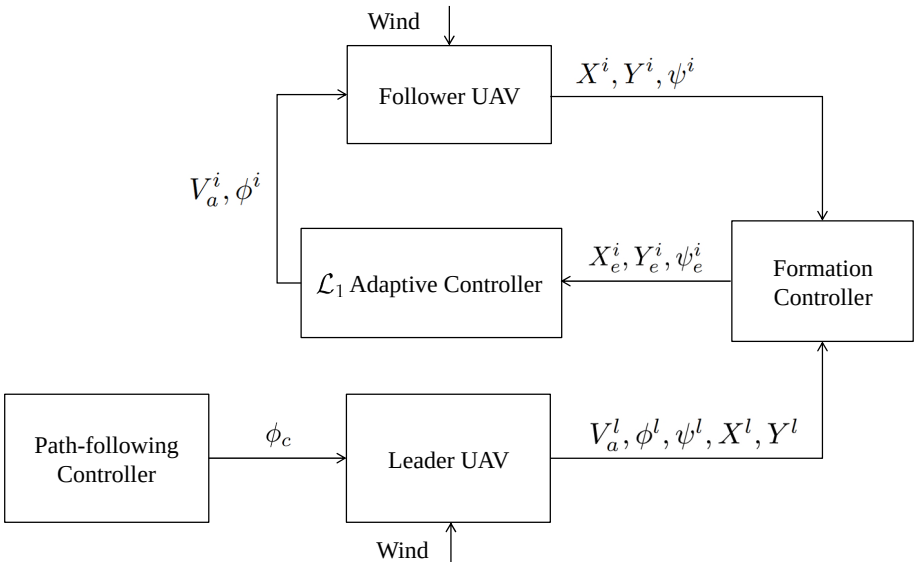

Fig. 2 $\mathcal{L}_1$ adaptive formation control in wind.

$\mathcal{L}_1$ adaptive control is a suitable approach for systems subject to external time-varying disturbances, such as small UAVs motion in wind. This is due to its fast and robust adaptation that leads to desired transient performance for both system input and output [29].

3 $\mathcal{L}_1$ Adaptive Formation Control

In adaptive control design, a common practice is to linearize a nonlinear model at an operating point to create a linear controller. This linear controller is then combined with an adaptive controller, leveraging prior system knowledge to enhance system robustness [41].

For the equilibrium point $(0, 0, 0, V_a^l, 0)$, the linearized state space model of equation (10) is given by

$$\dot{\bar{x}}^i = A_p \bar{x}^i + B_p \bar{u}^i, \tag{11}$$

where

$$A_p = \begin{pmatrix} 0 & 0 & 0 \\ 0 & 0 & V_a^l \\ 0 & 0 & 0 \end{pmatrix} \text{ and } B_p = \begin{pmatrix} -1 & 0 \\ 0 & 0 \\ 0 & -g/V_a^l \end{pmatrix}.$$

Hence, the non-linear system of (9) can be written as follows

$$\dot{x}^i = A_p x^i + B_p u^i + \tilde{f}^i, \tag{12}$$

where $\tilde{f}^i(x^i, u^i, t)$ is a nonlinear function that includes the higher order terms of the Taylor series expansion of $f(x^i, u^i)$ and the external disturbance $d^i(t)$.

Remark 3. It is important to underline that the matrices A_p and B_p are uncertain because it is not possible for the leader UAV, in real flight conditions, to maintain a constant airspeed V_a^l and consequently a constant heading rate $w^l = (g/V_a^l)\tan\phi^l$. This is especially true in the presence of wind.

The system of (12) can be written as

$$\dot{x}^i = A_m^i x^i + B\,\omega^i\,u^i + (A_p - A_m^i)x^i + \tilde{f}^i, \tag{13}$$

where $A_m^i = A_p - B\,K_p^i$ are Hurwitz matrices of the desired dynamics of the system, B is the input matrix of the system with the nominal airspeed of the leader UAV, $K_p^i \in \mathbb{R}^{2\times 3}$ are the feedback matrices, and $\omega^i \in \mathbb{R}^{2\times 2}$ are matrices of unknown parameters.

Remark 4. Choosing different desired dynamics for each follower UAV will give better flexibility for the design of the system. However, a simpler approach would be that the desired dynamics of the followers are chosen to be the same.

For control design, the following approximation can be used

$$(A_p - A_m^i)x^i + \tilde{f}^i = B\left(\theta^i x^i + \eta_m^i\right) + \eta_u^i, \tag{14}$$

where $\theta^i \in \mathbb{R}^{2\times 3}$ are matrices of unknown parameters, $\eta_m^i(t) \in \mathbb{R}^2$ are vectors of matched disturbances and $\eta_u^i(t) \in \mathbb{R}^3$ are vectors of unmatched disturbances.

Consequently, the system of (13) can be written as follows

$$\dot{x}^i = A_m^i x^i + B\left(\omega^i\,u^i + \theta^i x^i + \eta_m^i\right) + \eta_u^i. \tag{15}$$

The resulting model makes it straightforward to apply $\mathcal{L}_1$ adaptive control.

Remark 5. The main advantage of the application of $\mathcal{L}_1$ adaptive control to UAV formation control in wind is that good performance of the system can be obtained, whether the unknown wind speed is constant or not. This is a direct consequence of what was demonstrated in [29, 42] that the $\mathcal{L}_1$ adaptive controller presents a good compromise between performance and robustness in the presence of external disturbances.

Assumption 6. The unknown model parameters θ^i and the external unmatched disturbances σ^i are bounded, i.e., $\theta^i \in \Theta$ and $\sigma_i \in \Delta$, where Θ and Δ are known compact convex sets. The system input matrices ω^i are assumed to be unknown (non-singular) strictly row-diagonally dominant matrices with $\mathrm{sgn}(\omega_{ii}^i)$ assumed to be known. Also, it is assumed that there exists a known compact convex set Ω such that $\omega^i \in \Omega \subset \mathbb{R}^{2\times 2}$.

Assumption 7. It is also assumed that θ^i and σ^i are differentiable with bounded derivatives, i.e. there exist finite d_θ and d_σ such that

$$\sqrt{\mathrm{tr}(\dot{\theta}^{i\top}\dot{\theta}^i)} \leq d_\theta, \quad \|\dot{\sigma}^i\|_2 \leq d_\sigma.$$

The objective is to design a state-feedback controller for every agent i in order to ensure that the output of each UAV tracks a given piecewise continuous bounded reference signal $r^i(t)$.

4 $\mathcal{L}_1$ adaptive controller of MIMO systems with disturbances of unknown bounds

In this section, based on [37], the $\mathcal{L}_1$ adaptive controller for SISO systems with disturbances of unknown bounds [42] is extended to MIMO systems. This control approach draws insights from sliding mode control to design the adaptive laws. The main advantage is that the estimation of both the disturbances and their bounds is achieved by using a sliding surface. Consequently, the performance and robustness of the control system improve without assuming prior information about external perturbations.

4.1 Controller Design

As shown in Fig. 3, the $\mathcal{L}_1$ adaptive controller consists of three components: the state predictor, the adaptive law with fast adaptation, and the control law with a low-pass filter [29]. The state predictor is a designed dynamic system that contains a vector of adaptive parameters. The adaptive law is used to update adaptive parameters such that the error between the predicted state and the real state is small enough. The control law is designed to ensure that the output tracks any given references. Using this structure the $\mathcal{L}_1$ adaptive controller ensures robust tracking performance with fast adaptation.

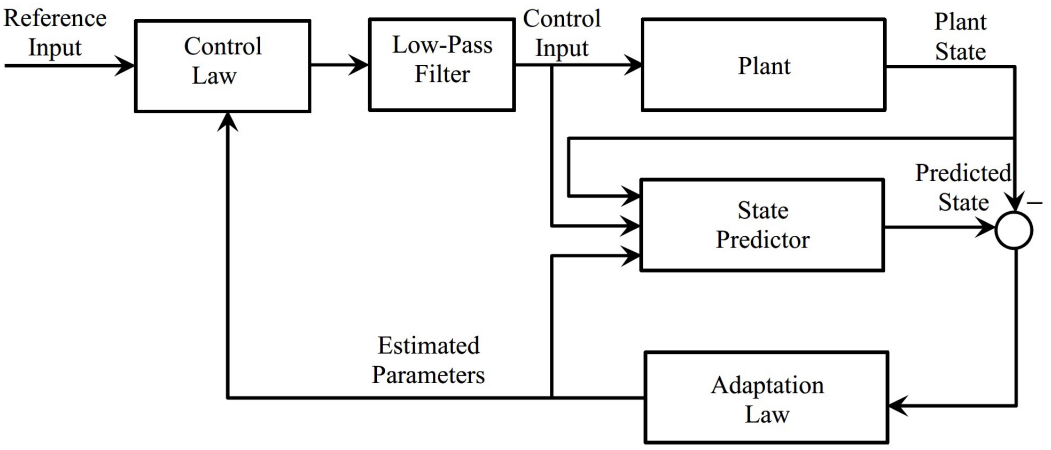

Fig. 3 General architecture of the $\mathcal{L}_1$ adaptive controller.

The model in (15) is equivalent to the class of MIMO systems defined by

$$\begin{aligned} \dot{x}(t) &= A_m x(t) + B\big(\omega u(t) + \theta^\top x(t) + \eta_m(t)\big) + \eta_u(t,x), \\ y(t) &= Cx(t), \quad x(0) = x_0, \end{aligned} \tag{16}$$

where $A_m \in \mathbb{R}$ is a known Hurwitz matrix that defines the desired dynamics of the system; $B^{n\times m}$, $C \in \mathbb{R}^{m\times n}$ are known constant matrices; $x(t) \in \mathbb{R}^n$ is the state vector which is assumed available through measurement; $u(t) \in \mathbb{R}^m$ is the control input vector; $y(t) \in \mathbb{R}^m$ is the output vector; $\omega \in \mathbb{R}^{m\times m}$ is an unknown constant matrix; $\theta^\top \in \mathbb{R}^{m\times n}$ is a matrix of constant unknown parameters representing

model uncertainties; $\eta_m(t) \in \mathbb{R}^m$ is an unknown matched disturbance; and $\eta_u(t,x) \in \mathbb{R}^n$ is an unknown unmatched disturbance.

Assumption 8. The non-linear functions $\eta_m(t)$ and $\eta_u(t,x)$ are uniformly bounded, i.e., there exist unknown real constants $L_m > 0$ and $L_u > 0$, such that for all $t \geq 0$ the following bounds hold:

$$\|\eta_m(t)\| \leq L_m \text{ and } \|\eta_u(t,x)\| \leq L_u.$$

Assumption 9. The unknown model parameters are bounded, i.e., $\theta \in \Theta$, where Θ is a known compact convex set. The system input gain matrix ω is assumed to be an unknown (non-singular) strictly row-diagonally dominant matrix with $\text{sgn}(\omega_{ii})$ known. Also, it is assumed that there exists a known compact convex set Ω such that $\omega \in \Omega \subset \mathbb{R}^{m\times m}$.

4.2 Controller Design

The state predictor is defined as

$$\begin{aligned} \dot{\hat{x}}(t) &= A_m\hat{x}(t) + B\big(\hat{\omega}(t)u(t) + \hat{\theta}^\top(t)x(t) + \hat{\eta}_m(t)\big) + \hat{\eta}_u(t), \\ \hat{y}(t) &= C\hat{x}(t), \quad \hat{x}(0) = x_0, \end{aligned} \tag{17}$$

where $\hat{x}(t)$ is the predicted state and $\hat{\theta}(t)$, $\hat{\omega}(t)$, $\hat{\eta}_m(t)$, and $\hat{\eta}_u(t)$ are the estimates of the unknown system parameters and disturbances.

The sliding surface is defined as

$$\sigma(t) = \lambda\tilde{x}(t), \tag{18}$$

where $\tilde{x}(t) = \hat{x}(t) - x(t)$ is the state estimation error and $\lambda \in \mathbb{R}^{m\times n}$ is a constant arbitrary matrix, chosen such that λB is non-singular and the coefficients $\lambda(i,j) : i = 1..n; j = 1..m$ form a stable hyperplane.

The estimation of the matched disturbance $\eta_m(t)$ is defined by

$$\hat{\eta}_m(t) = -(\lambda B)^{-1}\big(\lambda A_m\tilde{x}(t) + \rho\sigma(t)\big) - \hat{L}_m(t)\frac{B^\top\lambda^\top\sigma(t)}{\|B^\top\lambda^\top\sigma(t)\|}, \tag{19}$$

where $\rho > 0$ is arbitrary and the estimated bound $\hat{L}_m(t)$ is given by

$$\dot{\hat{L}}_m(t) = \Gamma\|\sigma^\top(t)\lambda B\|, \; L_{m0} = \hat{L}_m(0), \tag{20}$$

where $\Gamma \in \mathbb{R}^+$ is the adaptation rate.

The estimation of the unmatched disturbance $\eta_u(t,x)$ is defined by

$$\hat{\eta}_u(t) = -\hat{L}_u(t)\frac{\lambda^\top\sigma(t)}{\|\lambda^\top\sigma(t)\|}, \tag{21}$$

where the estimated bound $\hat{L}_u(t)$ is computed by

$$\dot{\hat{L}}_u(t) = \Gamma\|\sigma^\top(t)\lambda\|, \; L_{u0} = \hat{L}_u(0). \tag{22}$$

The input gain matrix ω and unknown parameters matrix θ are estimated by

$$\begin{aligned} \dot{\hat{\omega}}(t) &= -\Gamma\,\text{Proj}\big(\hat{\omega}(t), u(t)\,\sigma^\top(t)\lambda\,B\big)^\top, \\ \dot{\hat{\theta}}(t) &= -\Gamma\,\text{Proj}\big(\hat{\theta}(t), x(t)\,\sigma^\top(t)\lambda\,B\big). \end{aligned} \tag{23}$$

The control law is given by

$$u(s) = K\,D(s)\Big(K_g\,r(s) - \hat{\nu}_1(s) - \hat{\nu}_2(s)\Big), \tag{24}$$

where $D(s)$ is an $m \times m$ strictly proper transfer matrix; $K \in \mathbb{R}^{m\times m}$; $K_g = -(CA_m^{-1}B)^{-1}$ is the pre-filter of the MIMO control law; $\hat{\nu}_1(s)$ is the Laplace transformation of $\hat{\nu}_1(t) = \hat{\theta}^\top(t)x(t) + \hat{\omega}(t)u(t) + \hat{\eta}_m(t)$; $H_m(s) = C(s\mathbb{I} - A_m)^{-1}B$; $H_0(s) = C(s\mathbb{I} - A_m)^{-1}$; and $\hat{\nu}_2 = H_m^{-1}(s)H_0(s)\hat{\eta}_u(s)$.

The design of $D(s)$ and K should lead to a strictly proper and stable filter transfer matrix

$$C(s) = \omega KD(s)(\mathbb{I} + \omega KD(s))^{-1},$$

with steady state DC gain $C(0) = \mathbb{I}$.

4.3 Controller Analysis

Let

$$L = \max_{\theta\in\Theta} \|\theta\|_1,\ H(s) = (s\mathbb{I} - A_m)^{-1}B,\ G(s) = H(s)\big(\mathbb{I} - C(s)\big). \tag{25}$$

The $\mathcal{L}_1$ adaptive controller defined via equations (17)-(24) is subject to the following $\mathcal{L}_1$ norm condition:

$$\|G(s)\|_{\mathcal{L}_1} L < 1. \tag{26}$$

Moreover, the design of $C(s)$ needs to ensure that the transfer matrix

$$G_u(s) = (s\mathbb{I} - A_m)^{-1} - H(s)C(s)H_m^{-1}(s)H_0(s), \tag{27}$$

is a proper and stable.

In the following it is shown that the closed loop reference system, i.e. the closed-loop system with nominal parameters, is stable. The reference system is defined by

$$\begin{aligned} \dot{x}_r(t) &= A_m x_r(t) + B\big(\omega u_r(t) + \theta^\top x_r(t) + \eta_m(t)\big) + \eta_u(t,x), \\ y_r(t) &= Cx_r(t), \qquad x_r(0) = x_0. \end{aligned} \tag{28}$$

The reference control law is given by

$$u_r(s) = \omega^{-1}C(s)\Big(K_g r(s) - \nu_{1r}(s) - \nu_{2r}(s)\Big), \tag{29}$$

where $\nu_{1r}(s)$ is the Laplace transformation of $\nu_{1r}(t) = \theta^\top x_r(t) + \eta_m(t)$ and $\nu_{2r} = H_m^{-1}(s)H_0(s)\eta_u(s)$.

Lemma 1. If the filter $C(s)$ is designed such that it verifies the $\mathcal{L}_1$ norm condition in (26) and the requirement in (27), then the closed-loop reference system in (28) and (29) is BIBS stable with respect to the reference input and initial conditions.

The proof is in the appendix.

In the following, it is stated that the prediction error $\tilde{x}(t)$, and the estimation errors of the disturbances, their bounds and the unknown parameters are uniformly bounded.

Lemma 2. The following bound holds for the norm of the prediction error

$$\|\tilde{x}\|_{\mathcal{L}_\infty} \le \delta, \tag{30}$$

where $\delta > 0$ is arbitrary small. Furthermore, if the closed-loop system is stable then the prediction error $\tilde{x}(t)$ converges to zero, i.e.,

$$\lim_{t\to\infty} \tilde{x}(t) = 0. \tag{31}$$

The proof is in the appendix.

Next, in the following theorem the performance bounds of the $\mathcal{L}_1$ adaptive controller are shown.

Theorem. Given the system (16), the reference system (28) and (29) and the $\mathcal{L}_1$ adaptive controller (17) to (24), we have

$$\|x_r - x\|_{\mathcal{L}_\infty} \leq \gamma_1, \tag{32}$$

$$\|u_r - u\|_{\mathcal{L}_\infty} \leq \gamma_2, \tag{33}$$

where

$$\gamma_1 = 2\frac{\|G(s)\|_{\mathcal{L}_1}}{1 - \|G(s)\|_{\mathcal{L}_1} L} L_m + 2\frac{\|G_u(s)\|_{\mathcal{L}_1}}{1 - \|G(s)\|_{\mathcal{L}_1} L} L_u + \frac{\|H(s)C(s)H_m^{-1}(s)C\|_{\mathcal{L}_1}}{1 - \|G(s)\|_{\mathcal{L}_1} L}\delta,$$

and

$$\gamma_2 = \|\omega^{-1}C(s)\|_{\mathcal{L}_1}\Big(L\gamma_1 + 2(L_m + \|H_m^{-1}(s)H_0(s)\|_{\mathcal{L}_1} L_u) + C(s)H_m^{-1}(s)\delta\Big).$$

The proof is in the appendix.

5 Simulation Results

In this section, the simulation results for the $\mathcal{L}_1$ adaptive and a linear path-following controllers are presented. The performance of the controllers was evaluated in two case scenarios: (1) in time-varying wind and (2) in a situation where the UAV airspeeds vary under wind effect.

First, the design of a Linear Quadratic Integral (LQI) controller for the system is is presented. The objective is to provide a comparison baseline for the performance evaluation of the $\mathcal{L}_1$ adaptive controller. For the design of the LQI controller, the regulated outputs errors, denoted by e_I^i, are considered for the linear system in (11). The augmented system can be written as

$$\begin{bmatrix} \dot{\bar{x}}^i \\ \dot{e}_I^i \end{bmatrix} = \begin{bmatrix} A_p & 0 \\ -C & 0 \end{bmatrix}\begin{bmatrix} \bar{x}^i \\ e_I^i \end{bmatrix} + \begin{bmatrix} B \\ 0 \end{bmatrix}\bar{u}^i, \tag{34}$$

where A is the system dynamics matrix for the nominal airspeed.

The control laws of the system are given by

$$\bar{u}^i = -K_p^i \bar{x}^i - K_I^i e_I^i, \tag{35}$$

where $K_I^i \in \mathbb{R}^{2\times 2}$ are the integral feedback vectors and $K_p^i \in \mathbb{R}^{2\times 2}$ are the proportional feedback vectors that are designed to obtain the same desired dynamics matrices as the $\mathcal{L}_1$ adaptive controller $A_m^i = A - B\,K_p^i$.

The state-feedback vectors K_p^i were computed by the Linear Quadratic Regulator (LQR) method. The transfer functions $D^i(s)$ of the $\mathcal{L}_1$ adaptive controllers was chosen as $D^i(s) = 1/(s(s+28))$ and $K^i = 36$, which leaded to filters $F^i(s) = 36/(s^2 + 8.4s + 36)$.

It is important to note that the same desired system dynamics and initialization parameters were used for both linear and adaptive controllers in order to provide a fair comparison.

The leader UAV was commanded to fly a straight-line path, defined by four waypoints, with the cross-track error d required to be zero. Two follower UAVs that were assigned to fly at distances ($X_d^1 = -20$ m, $Y_d^1 = 20$ m) and ($X_d^2 = -20$ m, $Y_d^2 = -20$ m), respectively. The initial positions of the leader and follower UAVs were at the earth frame origin.

The airspeed of the leader UAV was assumed to be regulated at 20 m/s. Gravity was $g = 9.81$ m/s^2. It was further assumed that the maximum turn angle magnitude of each UAV is $|\phi| = 60^\circ$ and the commanded airspeeds are within the interval $[5, 40]$ m/s.

Analysis in Case of no Wind

Simulation results show that both $\mathcal{L}_1$ adaptive and LQI controllers present satisfactory performance when there are no wind disturbances. The trajectories of the UAVs relative to the desired path are shown in Fig. 4. The cross-track and along-track errors, the heading error are illustrated in Fig. 5a. The commanded airspeeds and roll angles of the followers are illustrated in Fig. 5b. It can be observed that the $\mathcal{L}_1$ adaptive controller has performed slightly better than the LQI controller because it shows relatively smaller values in peak errors. This is obviously due to its fast adaptation in the presence of changing parameter uncertainties. The presence of peaks in the cross-track error is due to the rolling motion of the UAVs when turning at the waypoints.

.

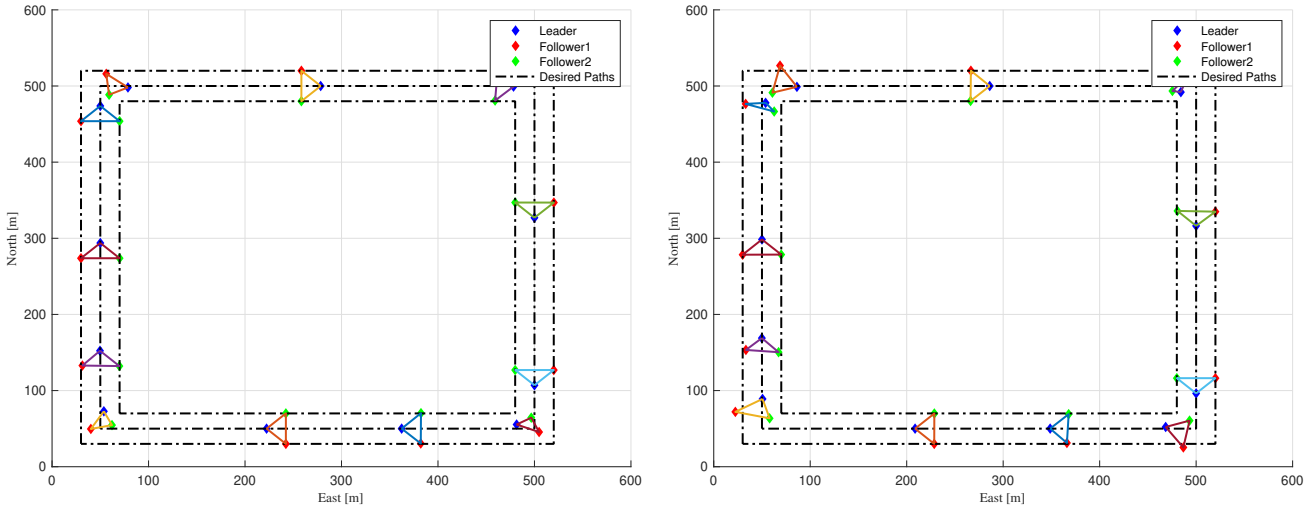

(a) $\mathcal{L}_1$ controller **(b) LQI Controller**

Fig. 4 UAV trajectories without wind.

Analysis in Case of Time-varying Wind

In the second simulations, a time-varying crosswind was introduced. Its velocity was assumed to be a periodic signal, $W_e(t) = 5 + 5\sin(2\pi t)$ m/s.

From Fig. 6 and Fig. 7a it can be noticed that the $\mathcal{L}_1$ adaptive controller performs better than the LQI controller in the same wind conditions. In particular, it can be noted that the trajectory of the UAVs are smoother and more precise with the $\mathcal{L}_1$ adaptive controller. Moreover, it is clearly illustrated that the cross-track error is not completely eliminated by the LQI controller. Fig. 7b also shows that the airspeed and roll commands exhibit less saturation with the $\mathcal{L}_1$ adaptive controller compared to the LQI controller.

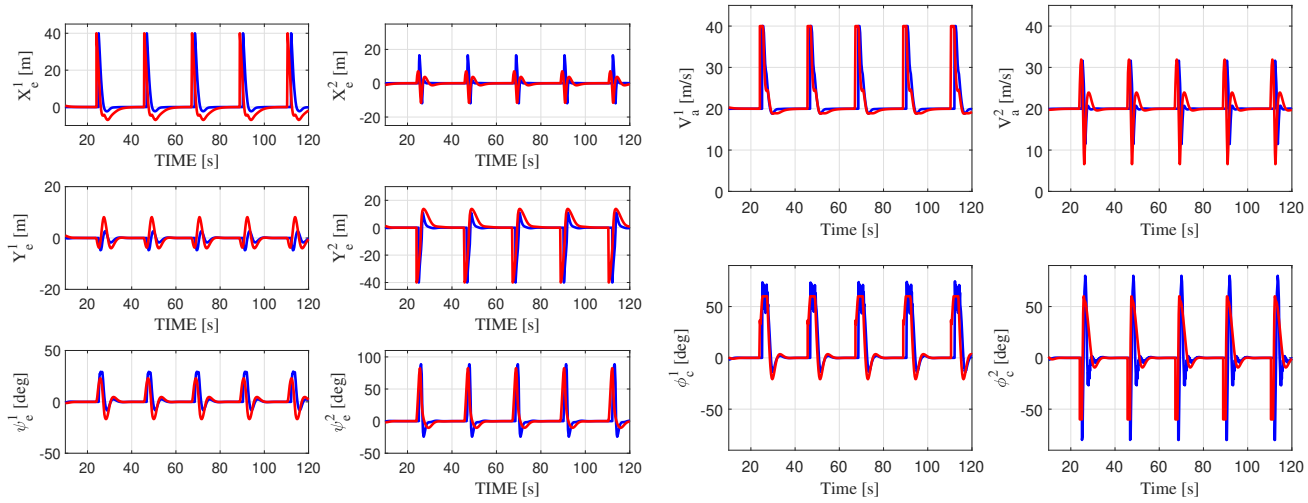

(a) Path-following errors **(b) Airspeed and roll command of the followers**

Fig. 5 Performance of the UAVs without wind ($\mathcal{L}_1$ blue, LQI red).

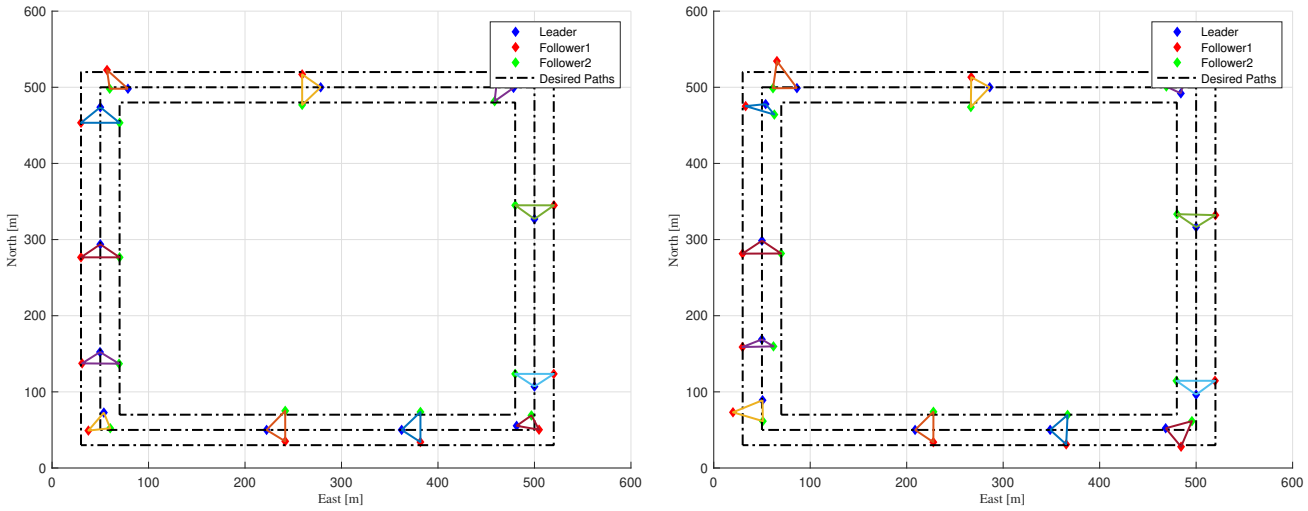

(a) $\mathcal{L}_1$ controller **(b) LQI Controller**

Fig. 6 UAV trajectories in time-varying wind.

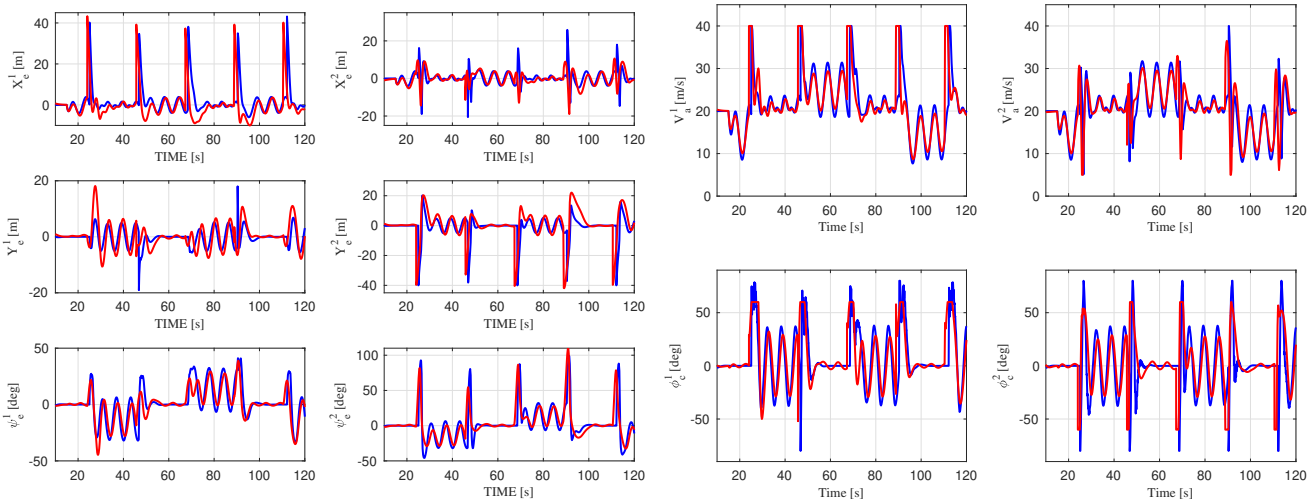

(a) Path-following errors **(b) Airspeed and roll Command the of the followers**

Fig. 7 Performance of the UAVs in time-varying wind ($\mathcal{L}_1$ blue, LQI red).

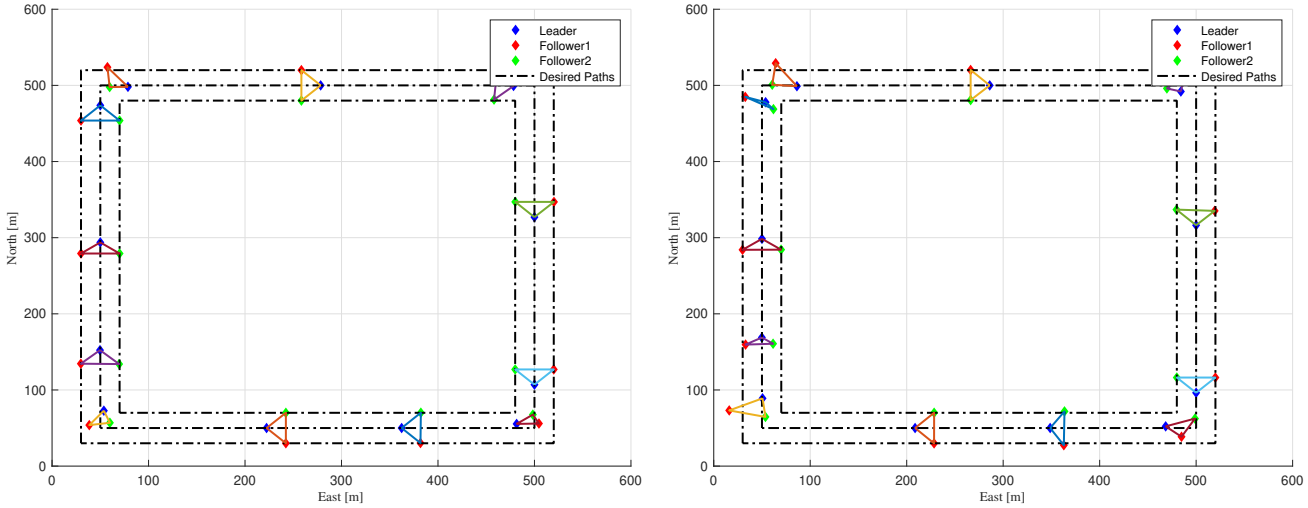

(a) $\mathcal{L}_1$ controller **(b) LQI Controller**

Fig. 8 UAV trajectories with leader varying airspeed.

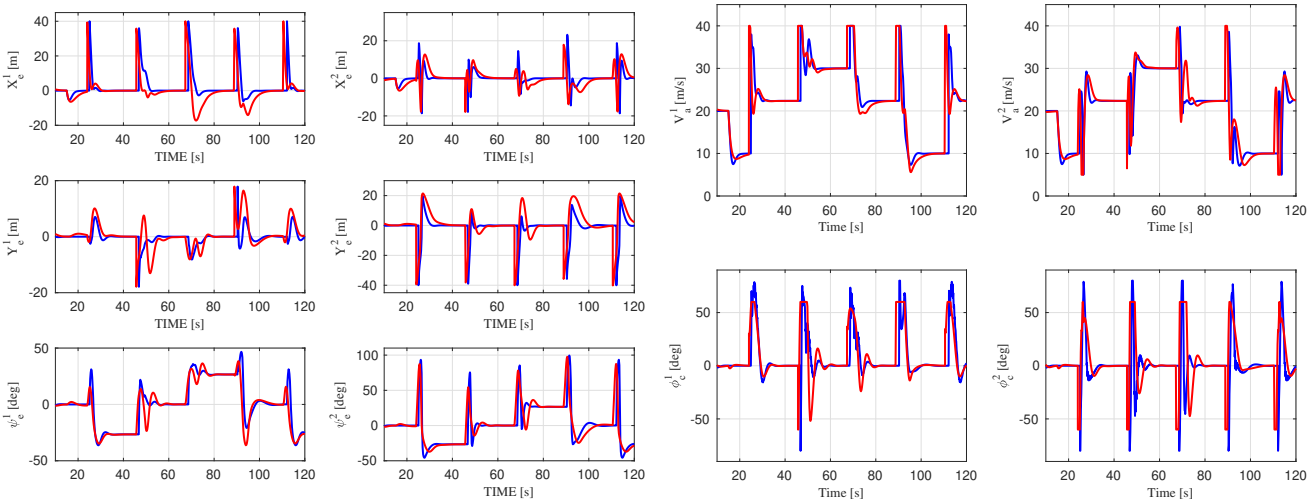

(a) Path-following errors **(b) Airspeed and roll command the of the followers**

Fig. 9 Performance of the UAVs with time-varying airspeed ($\mathcal{L}_1$ blue, LQI red).

Analysis in Case of Leader Varying Airspeed

A practical issue in UAV trajectory control, is that maintaining a constant airspeed for the leader is not feasible in practice, especially in the presence of wind disturbances [28].

In order to simulate this situation, a constant wind, with a speed of 10 m/s, blowing in the easterly direction is acting on the leader UAV. Hence, it was assumed that:

- The airspeed V_a^l increases by 3 m/s when the leader UAV is flying downwind.
- The airspeed V_a^l decreases by 3 m/s when the leader UAV is flying upwind
- The airspeed V_a^l decreases by 1 m/s when the leader UAV is flying crosswind.

This assumption does not have a flight mechanical justification. It is used only for simulation purposes. It was also assumed that the follower UAV is flying in an easterly wind with constant speed of 10 m/s.

It is shown in Fig. 8 that both controllers were able to keep the UAV on the desired path under variations of the airspeed. However Fig. 9a shows clearly that the long-track errors x_e and cross-track errors y_e converge quickly with the $\mathcal{L}_1$ adaptive controller, because of fast adaptation in the presence of

external disturbances and unknown parameters as consequence of the time-varying airspeed of the leader UAV. The commanded airspeeds and roll angles of the followers are illustrated in Fig. 9b. The airspeed and roll commands exhibit less saturation with the $\mathcal{L}_1$ adaptive controller compared to the LQI controller.

6 Conclusion

This paper presents a robust adaptive fixed-wing UAV formation controller designed to handle wind disturbances, explicitly accounting for the time-varying nature of wind speed. The core concept is to model the leader-follower formation of fixed-wing UAVs as a control design problem for systems affected by parametric uncertainties and external disturbances.

The proposed solution is based on the application of the $\mathcal{L}_1$ adaptive controller for MIMO systems. By considering the variability of wind speed in real-world scenarios, such as wind shear or wind gusts, the design becomes more realistic and the analysis more rigorous, ultimately enhancing the system robustness. While the design primarily focused on 2D straight paths, extending it to 3D curved paths is a straightforward endeavor.

Although the framework presented in this paper has been successfully demonstrated in simulations, it is imperative to validate it through real flight tests. Furthermore, taking into account that in reality, wind velocity is entirely unpredictable, being a stochastic phenomenon, offers a more realistic approach to the problem of UAV formation control under wind disturbances.

Future research directions may also explore the design based on a cascaded $\mathcal{L}_1$ adaptive architecture, with the inner controller based on $\mathcal{L}_1$ adaptive control. Analyzing the stability of such a system is a main theoretical challenge. Another avenue of investigation involves integrated guidance and control, merging both the outer-loop and the inner-loop within the same control loop of the UAVs. Moreover, formulating UAV formation control as a control design problem in the presence of uncertainties and external disturbances opens the door to a wide array of control methodologies for the development of robust path-following in windy conditions.

Appendix

Proof of Lemma 1. The closed-loop reference system (28) and (29) can be written

$$x_r(s) = H(s)C(s)K_g r(s) + G(s)\theta^\top x_r(s) + G(s)\eta_m(s) + G_u(s)\eta_u(s) + x_{in}(s), \tag{36}$$

where $x_{in}(s) = (s\mathbb{I} - A_m)^{-1}x_0$. Then, for all $t \in [0, \tau]$ we have

$$\begin{aligned}\|x_{r_\tau}\|_{\mathcal{L}_\infty} \leq &\|H(s)C(s)\|_{\mathcal{L}_1}K_g\|r_\tau\|_{\mathcal{L}_\infty} + \|G(s)\|_{\mathcal{L}_1}L\|x_{r_\tau}\|_{\mathcal{L}_\infty} \\ &+ \|G(s)\|_{\mathcal{L}_1}\|\eta_{m_\tau}\|_{\mathcal{L}_\infty} + \|G_u(s)\|_{\mathcal{L}_1}\|\eta_{u_\tau}\|_{\mathcal{L}_\infty} + \|x_{in_\tau}\|_{\mathcal{L}_\infty}\end{aligned} \tag{37}$$

Substituting the upper bounds of η_m and η_u and solving for $\|x_{r_\tau}\|_{\mathcal{L}_\infty}$ in the equation above to obtain the following bound

$$\|x_{r_\tau}\|_{\mathcal{L}_\infty} \leq \frac{\|H(s)C(s)\|_{\mathcal{L}_1}K_g\|r_\tau\|_{\mathcal{L}_\infty} + \|G(s)\|_{\mathcal{L}_1}L_m}{1 - \|G(s)\|_{\mathcal{L}_1}L} + \frac{\|G_u(s)\|_{\mathcal{L}_1}L_u + \|x_{in}\|_{\mathcal{L}_\infty}}{1 - \|G(s)\|_{\mathcal{L}_1}L}. \tag{38}$$

If the $\mathcal{L}_1$ norm condition in (26) is verified then $\|x_{r_\tau}\|_{\mathcal{L}_\infty}$ is uniformly bounded for all $\tau > 0$, and the proof is complete. □

Proof of Lemma 2.

From (16) and (17), the prediction error dynamics can be written

$$\dot{\tilde{x}} = A_m\tilde{x} + B\big(\tilde{\omega}u + \tilde{\theta}^\top x + \tilde{\eta}_m\big) + \tilde{\eta}_u. \tag{39}$$

Consider the Lyapunov function candidate

$$V = \frac{1}{2}\sigma^\top\sigma + \frac{1}{2}\Gamma^{-1}\Big(\mathrm{tr}\big(\tilde{\theta}^\top\tilde{\theta}\big) + \mathrm{tr}\big(\tilde{\omega}^\top\tilde{\omega}\big) + \tilde{L}_m^2 + \tilde{L}_u^2\Big), \tag{40}$$

whose derivative is given by

$$\dot{V} = \sigma^\top\dot{\sigma} + \Gamma^{-1}\Big(\mathrm{tr}\big(\tilde{\theta}^\top\dot{\tilde{\theta}}\big) + \mathrm{tr}\big(\tilde{\omega}^\top\dot{\tilde{\omega}}\big) + \tilde{L}_m\dot{\tilde{L}}_m + \tilde{L}_u\dot{\tilde{L}}_u\Big). \tag{41}$$

From (18) and (39) the derivative of the sliding surface can be written

$$\dot{\sigma} = \lambda A_m\tilde{x} + \lambda B\big(\tilde{\theta}^\top x + \tilde{\omega}u + \tilde{\eta}_m\big) + \lambda\tilde{\eta}_u. \tag{42}$$

Substituting into (41), we get

$$\begin{aligned}\dot{V} =&\sigma^\top\Big(\lambda A_m\tilde{x} + \lambda B\big(\tilde{\theta}^\top x + \tilde{\omega}u + (\hat{\eta}_m - \eta_m)\big) + \lambda(\hat{\eta}_u - \eta_u)\Big)\\ &+ \Gamma^{-1}\big(\mathrm{tr}\big(\tilde{\theta}^\top\dot{\tilde{\theta}}\big) + \mathrm{tr}\big(\tilde{\omega}^\top\dot{\tilde{\omega}}\big) + \tilde{L}_m\dot{\tilde{L}}_m + \tilde{L}_u\dot{\tilde{L}}_u\big).\end{aligned} \tag{43}$$

Given the fact that for any scalar s, $\mathrm{tr}(s) = s$, hence

$$\begin{aligned}\dot{V} =&\sigma^\top\lambda A_m\tilde{x} + \mathrm{tr}(\sigma^\top\lambda B\tilde{\theta}^\top x) + \mathrm{tr}(\sigma^\top\lambda B\tilde{\omega}u) + \sigma^\top\lambda B(\hat{\eta}_m - \eta_m) + \sigma^\top\lambda(\hat{\eta}_u - \eta_u)\\ &+ \Gamma^{-1}\big(\mathrm{tr}\big(\tilde{\theta}^\top\dot{\tilde{\theta}}\big) + \mathrm{tr}\big(\tilde{\omega}^\top\dot{\tilde{\omega}}\big) + \tilde{L}_m\dot{\tilde{L}}_m + \tilde{L}_u\dot{\tilde{L}}_u\big).\end{aligned} \tag{44}$$

Using the property $\mathrm{tr}(XY) = \mathrm{tr}(YX)$ for any matrices X, Y, we obtain

$$\begin{aligned}\dot{V} =&\sigma^\top\lambda A_m\tilde{x} + \mathrm{tr}(\tilde{\theta}^\top x\sigma^\top\lambda B) + \mathrm{tr}(\tilde{\omega}u\sigma^\top\lambda B) + \sigma^\top\lambda B(\hat{\eta}_m - \eta_m) + \sigma^\top\lambda(\hat{\eta}_u - \eta_u)\\ &+ \Gamma^{-1}\big(\mathrm{tr}\big(\tilde{\theta}^\top\dot{\tilde{\theta}}\big) + \mathrm{tr}\big(\tilde{\omega}^\top\dot{\tilde{\omega}}\big) + \tilde{L}_m\dot{\tilde{L}}_m + \tilde{L}_u\dot{\tilde{L}}_u\big).\end{aligned} \tag{45}$$

Given $\hat{\eta}_m$ and $\hat{\eta}_u$ from (19) and (21) and the adaptation law (23) it can be written

$$\dot{V} = -\rho\sigma^\top\sigma - \sigma^\top\lambda B\eta_m - \sigma^\top\lambda\eta_u - \|\sigma^\top\lambda B\|\hat{L}_m - \|\sigma^\top\lambda\|\hat{L}_u + \Gamma^{-1}\big(\tilde{L}_m\dot{\tilde{L}}_m + \tilde{L}_u\dot{\tilde{L}}_u\big). \tag{46}$$

Hence, the following upper bound can be derived

$$\dot{V} \leq -\rho\|\sigma\|^2 + \|\sigma^\top\lambda B\|\|\eta_m\| + \|\sigma^\top\lambda\|\|\eta_u\| - \|\sigma^\top\lambda B\|\hat{L}_m - \|\sigma^\top\lambda\|\hat{L}_u + \Gamma^{-1}\big(\tilde{L}_m\dot{\tilde{L}}_m + \tilde{L}_u\dot{\tilde{L}}_u\big). \tag{47}$$

Using Assumption 9, it follows that

$$\dot{V} \leq -\rho\|\sigma\|^2 - \|(\lambda B)^\top\sigma\|\tilde{L}_m - \|\lambda^\top\sigma\|\tilde{L}_u + \Gamma^{-1}\big(\tilde{L}_m\dot{\tilde{L}}_m + \tilde{L}_u\dot{\tilde{L}}_u\big). \tag{48}$$

Considering the adaptation laws from (20) and (22), it follows that

$$\dot{V} \leq -\rho\|\sigma\|^2. \tag{49}$$

Therefore, the sliding surface σ, the estimation errors of the unknown parameters $\tilde{\theta}$ and $\tilde{\omega}$; and the disturbance bound errors $\tilde{L}_m$ and $\tilde{L}_u$ are uniformly bounded. Consequently, the estimation errors of the external disturbances $\tilde{\eta}_m$ and $\tilde{\eta}_u$ are also uniformly bounded.

Since the coefficients of the sliding surface form a stable hyperplane and $\tilde{x}(0) = 0$, i.e., the system is initialized on the sliding surface, and given that on the sliding surface the trajectories are governed by $\sigma(\tilde{x}, t) = 0$, there always exists an arbitrarily small real $\delta > 0$ verifying

$$\|\tilde{x}\|_{\mathcal{L}_\infty} \leq \delta. \tag{50}$$

This result comes from the fundamental propriety of sliding mode control, stipulating that if the system is on the sliding surface, it stays on the nearby sliding surface despite disturbances [43].

Moreover, from (49) it can be written

$$\int_0^t \|\sigma(t)\|^2 dt \leq \frac{1}{\rho}\Big(V(0) - V(t)\Big). \tag{51}$$

Since $V(0)$ is bounded and $V(t)$ is bounded and non-increasing, therefore

$$\lim_{t\to\infty} \int_0^t \sigma(t)^2 dt \tag{52}$$

is bounded.

If the closed-loop system is stable, i.,e., $u(t)$ and $x(t)$ are bounded then $\dot{\sigma}(t)$ in (42) is bounded. By applying Barbalt's Lemma it follows that

$$\lim_{t\to\infty} \|\sigma(t)\|^2 = 0 \text{ and } \lim_{t\to\infty} \|\sigma(t)\| = 0. \tag{53}$$

Consequently

$$\lim_{t\to\infty} \tilde{x}(t) = 0, \tag{54}$$

and the proof is complete. □

Proof of the Theorem.

The control law in (24) can be written as

$$\begin{aligned} u(s) =& K\, D(s)\Big(K_g r(s) - \omega u(s) - \theta^\top x(s) - \eta_m(s)\Big) \\ & - K\, D(s)\Big(H_m^{-1}(s)H_0(s)\big(\eta_u(s) + \tilde{\eta}_u(s)\big) - \tilde{\nu}(s)\Big), \end{aligned} \tag{55}$$

where $\tilde{\nu}(s)$ is the Laplace transformation of $\tilde{\nu}(t) = \tilde{\omega}u(t) + \tilde{\theta}x(t) + \tilde{\eta}_m(t)$ and $\tilde{\eta}_u(s)$ is the Laplace transformation $\tilde{\eta}_u(t)$. Consequently

$$\begin{aligned} u(s) =& K\, D(s)\Big(\mathbb{I} + \omega K D(s)\Big)^{-1}\Big(K_g r(s) - \theta^\top x(s) - \eta_m(s)\Big) \\ & - K\, D(s)\Big(\mathbb{I} + \omega K D(s)\Big)^{-1}\Big(H_m^{-1}(s)H_0(s)\big(\eta_u(s) + \tilde{\eta}_u(s)\big) - \tilde{\nu}(s)\Big), \end{aligned}$$

which leads to

$$u(s) = \omega^{-1}C(s)\Big(K_g r(s) - \theta^\top x(s) - \eta_m(s)\Big) - \omega^{-1}C(s)\Big(H_m^{-1}(s)H_0(s)\big(\eta_u(s) + \tilde{\eta}_u(s)\big) - \tilde{\nu}(s)\Big). \tag{56}$$

Hence, the Laplace transformation of the closed loop system (16) and (56) can be written

$$\begin{aligned} x(s) =& H(s)C(s)K_g r(s) + G(s)\theta^\top x(s) + G(s)\eta_m(s) + G_u(s)\eta_u(s) \\ & - H(s)C(s)\big(\tilde{\nu}(s) + H_m^{-1}(s)H_0(s)\tilde{\eta}_u(s)\big) + x_{in}(s). \end{aligned} \tag{57}$$

Taking the difference of (36) and (57) it follows that

$$\begin{aligned} x_r(s) - x(s) =& G(s)\theta^\top (x_r(s) - x(s)) + G(s)\big(\eta_m(s) - \eta_{mr}(s)\big) + G_u(s)\big(\eta_u(s) - \eta_{ur}(s)\big) \\ &+ H(s)C(s)\big(\tilde{\nu}(s) + H_m^{-1}(s)H_0(s)\tilde{\eta}_u(s)\big). \end{aligned} \tag{58}$$

From (39) the Laplace transformation of the prediction error dynamics can be written

$$\tilde{x}(s) = H(s)\tilde{\nu}(s) + (s\mathbb{I} - A_m)^{-1}\tilde{\eta}_u(s). \tag{59}$$

Multiplying both terms of (59) by $H_m^{-1}(s)C$ gives

$$H_m^{-1}(s)C\tilde{x}(s) = \tilde{\nu}(s) + H_m^{-1}(s)H_0(s)\tilde{\eta}_u(s). \tag{60}$$

Substituting into (58) it follows that

$$\begin{aligned} x_r(s) - x(s) =& G(s)\theta^\top (x_r(s) - x(s)) + G(s)\big(\eta_m(s) - \eta_{mr}(s)\big) \\ &+ G_u(s)\big(\eta_u(s) - \eta_{ur}(s)\big) + H(s)C(s)H_m^{-1}(s)C\tilde{x}(s). \end{aligned} \tag{61}$$

Solving for $x_r(s) - x(s)$, the following bound holds for $t \in [0, \tau]$

$$\begin{aligned} \|(x_r - x)_\tau\|_{\mathcal{L}_\infty} \leq \frac{\|G(s)\|_{\mathcal{L}_1}}{1 - \|G(s)\|_{\mathcal{L}_1}L}\|(\eta_{m_\tau} - \eta_{mr})_\tau\|_{\mathcal{L}_\infty} + \frac{\|G_u(s)\|_{\mathcal{L}_1}}{1 - \|G(s)\|_{\mathcal{L}_1}L}\|(\eta_u - \eta_{ur})_\tau\|_{\mathcal{L}_\infty} \\ + \frac{\|H(s)C(s)H_m^{-1}(s)C\|_{\mathcal{L}_1}}{1 - \|G(s)\|_{\mathcal{L}_1}L}\|\tilde{x}_\tau\|_{\mathcal{L}_\infty}. \end{aligned} \tag{62}$$

Given the upper bound of $\tilde{x}(t)$ from Lemma 2.4, and the disturbance bounds from Assumption 9, it follows that

$$\begin{aligned} \|(x_r - x)_\tau\|_{\mathcal{L}_\infty} \leq 2\frac{\|G(s)\|_{\mathcal{L}_1}}{1 - \|G(s)\|_{\mathcal{L}_1}L}L_m + 2\frac{\|G_u(s)\|_{\mathcal{L}_1}}{1 - \|G(s)\|_{\mathcal{L}_1}L}L_u \\ + \frac{\|H(s)C(s)H_m^{-1}(s)C\|_{\mathcal{L}_1}}{1 - \|G(s)\|_{\mathcal{L}_1}L}\delta, \end{aligned} \tag{63}$$

which leads to the bound in (32).

To show the second bound in (33), by taking the difference of (29) and (56), we can derive

$$\begin{aligned} u_r(s) - u(s) =& -\omega^{-1}C(s)\theta^\top\Big(\big(x_r(s) - x(s)\big)\Big) - \omega^{-1}C(s)\big(\eta_m(s) - \eta_{mr}(s)\big) \\ &- \omega^{-1}C(s)H_m^{-1}(s)H_0(s)\big(\eta_u(s) - \eta_{ur}(s)\big) + \omega^{-1}C(s)\big(H_m^{-1}(s)H_0(s)(s)\tilde{\eta}_u(s) + \tilde{\nu}(s)\big). \end{aligned} \tag{64}$$

Hence

$$\begin{aligned} u_r(s) - u(s) =& -\omega^{-1}C(s)\theta^\top\Big(\big(x_r(s) - x(s)\big)\Big) - \omega^{-1}C(s)\big(\eta_m(s) - \eta_{mr}(s)\big) \\ &- \omega^{-1}C(s)H_m^{-1}(s)H_0(s)\big(\eta_u(s) - \eta_{ur}(s)\big) + \omega^{-1}C(s)H_m^{-1}(s)C(s)\tilde{x}(s), \end{aligned} \tag{65}$$

and (64) can be upper bounded as

$$\begin{aligned} \|(u_r - u)_\tau\|_{\mathcal{L}_\infty} \leq \|\omega^{-1}C(s)\|_{\mathcal{L}_1}L\|(x_r - x)_\tau\|_{\mathcal{L}_\infty} + 2\|\omega^{-1}C(s)\|_{\mathcal{L}_1}(L_m + \|H_m^{-1}(s)H_0(s)\|_{\mathcal{L}_1}L_u) \\ + \|\omega^{-1}C(s)\|_{\mathcal{L}_1}\|C(s)H_m^{-1}(s)C(s)\|_{\mathcal{L}_1}\|\tilde{x}_\tau\|_{\mathcal{L}_\infty}, \end{aligned} \tag{66}$$

which holds uniformly for all $\tau \geq 0$, leading to the bound in (33). □

References

[1] Randal W. Beard and Timothy W. McLain. *Small Unmanned Aircraft: Theory and Practice*. Princeton University Press, 2012.

[2] Reg Austin. *Unmanned Aircraft Systems: UAVs Design, Development and Deployment*, volume 54. John Wiley, 2011.

[3] Mostafa Hassanalian and Abdessattar Abdelkefi. Classifications, applications, and design challenges of drones: A review. *Progress in Aerospace Sciences*, 91:99–131, 2017.

[4] Francesco Nex, Costas Armenakis, Michael Cramer, Davide A. Cucci, Markus Gerke, Eija Honkavaara, Antero Kukko, Claudio Persello, and Jan Skaloud. UAV in the advent of the twenties: Where we stand and what is next. *ISPRS Journal of Photogrammetry and Remote Sensing*, 184:215–242, 2022.

[5] A. A. Laghari, A. K. Jumani, R. A. Laghari, and H. Nawaz. Unmanned aerial vehicles: A review. *Cognitive Robotics*, 3:8–22, 2023. ISSN: 2667-2413. DOI: https://doi.org/10.1016/j.cogr.2022.12.004.

[6] Syed Agha Hassnain Mohsan, Nawaf Qasem Hamood Othman, Yanlong Li, Mohammed H. Alsharif, and Muhammad Asghar Khan. Unmanned aerial vehicles (UAVs): Practical aspects, applications, open challenges, security issues, and future trends. *Intelligent Service Robotics*, 16(1):109–137, 2023.

[7] Osim Kumar Pal, Md Sakib Hossain Shovon, MF Mridha, and Jungpil Shin. A comprehensive review of ai-enabled unmanned aerial vehicle: Trends, vision, and challenges. *arXiv preprint arXiv:2310.16360*, 2023.

[8] Muhammad Amir Tahir, Imran Mir, and Tauqeer Ul Islam. A review of UAV platforms for autonomous applications: comprehensive analysis and future directions. *IEEE Access*, 11:52540–52554, 2023. DOI: 10.1109/ACCESS.2023.3273780.

[9] Christopher Heintz, Sean C. Bailey, and Jesse Hoagg. Formation control of fixed-wing unmanned aircraft: theory and experiments. In *AIAA Scitech 2019 Forum*, page 1168, 2019.

[10] Brandon J. Wellman and Jesse B. Hoagg. A flocking algorithm with individual agent destinations and without a centralized leader. *Systems & Control Letters*, 102:57–67, 2017.

[11] Giuliano Punzo, Philippos Karagiannakis, Derek J. Bennet, Malcolm Macdonald, and Stephan Weiss. Enabling and exploiting self-similar central symmetry formations. *IEEE Transactions on Aerospace and Electronic Systems*, 50(1):689–703, 2014.

[12] Yutaka Kanayama, Yoshihiko Kimura, Fumio Miyazaki, and Tetsuo Noguchi. A stable tracking control method for a non-holonomic mobile robot. In *IEEE/RSJ International Workshop on Intelligent Robots and Systems (IROS 91)*, pages 1236–1241. IEEE, 1991.

[13] Xiangke Wang, Yangguang Yu, and Zhongkui Li. Distributed sliding mode control for leader-follower formation flight of fixed-wing unmanned aerial vehicles subject to velocity constraints. *International Journal of Robust and Nonlinear Control*, 31(6):2110–2125, 2021.

[14] Cezary Kownacki and Leszek Ambroziak. Flexible structure control scheme of a UAVs formation to improve the formation stability during maneuvers. *Acta Mechanica et Automatica*, 11(3):178–185, 2017. DOI: 10.1515/ama-2017-0026.

[15] Wei Ren and Randy W. Beard. Trajectory tracking for unmanned air vehicles with velocity and heading rate constraints. *IEEE Transactions on Control Systems Technology*, 12(5):706–716, 2004. DOI: 10.1109/TCST.2004.826956.

[16] Fabrizio Giulietti, Lorenzo Pollini, and Mario Innocenti. Autonomous formation flight. *IEEE Control Systems Magazine*, 20(6):34–44, 2000.

[17] Z. X. Liu, X. Yu, C. Yuan, and Y. M. Zhang. Leader-follower formation control of unmanned aerial vehicles with fault tolerant and collision avoidance capabilities. In *2015 International Conference on Unmanned Aircraft Systems (ICUAS)*, pages 1025–1030. IEEE, 2015.

[18] Sai-Ming Li, Raman Mehra, and Jovan Boskovic. Globally stable automatic formation flight control in two dimensions. In *AIAA Guidance, Navigation, and Control Conference and Exhibit*, page 4046, 2001.

[19] E. Semsar and K. Khorasani. Adaptive formation control of UAVs in the presence of unknown vortex forces and leader commands. In *2006 American Control Conference*, pages 6–pp. IEEE, 2006.

[20] Damien Galzi and Yuri Shtessel. UAV formations control using high order sliding modes. In *2006 American Control Conference*, 2006. DOI: 10.1109/ACC.2006.1657386.

[21] Hamed Rezaee, Farzaneh Abdollahi, and Mohammad Bagher Menhaj. Model-free fuzzy leader-follower formation control of fixed wing UAVs. In *13th Iranian Conference on Fuzzy Systems (IFSC)*, pages 1–5. IEEE, 2013. DOI: 10.1109/IFSC.2013.6675677.

[22] Mohammad A. Dehghani and Mohammad B. Menhaj. Integral sliding mode formation control of fixed-wing unmanned aircraft using seeker as a relative measurement system. *Aerospace Science and Technology*, 58:318–327, 2016.

[23] Ziyang Zhen, Gang Tao, Yue Xu, and Ge Song. Multivariable adaptive control based consensus flight control system for UAVs formation. *Aerospace Science and Technology*, 93:105336, 2019. DOI: 10.1016/j.ast.2019.105336.

[24] Hai T. Do, Hoang T. Hua, Minh T. Nguyen, Cuong V. Nguyen, Hoa TT Nguyen, Hoa T Nguyen, and Nga TT Nguyen. Formation control algorithms for multiple-UAVs: a comprehensive survey. *EAI Endorsed Transactions on Industrial Networks and Intelligent Systems*, 8(27):e3–e3, 2021.

[25] Quan Ouyang, Zhaoxiang Wu, Yuhua Cong, and Zhisheng Wang. Formation control of unmanned aerial vehicle swarms: A comprehensive review. *Asian Journal of Control*, 25(1):570–593, 2023.

[26] Derek R. Nelson, D. Blake Barber, Timothy W. McLain, and Randal W. Beard. Vector field path following for miniature air vehicles. *IEEE Transactions on Robotics*, 23(3):519–529, 2007.

[27] Ximan Wang, Simone Baldi, Xuewei Feng, Changwei Wu, Hongwei Xie, and Bart De Schutter. A fixed-wing UAV formation algorithm based on vector field guidance. *IEEE Transactions on Automation Science and Engineering*, 20(1):179–192, 2022.

[28] Toufik Souanef. $\mathcal{L}_1$ adaptive path-following of small fixed-wing unmanned aerial vehicles in wind. *IEEE Transactions on Aerospace and Electronic Systems*, 58(4):3708–3716, 2022. DOI: 10.1109/TAES.2022.3153758.

[29] Naira Hovakimyan and Chengyu Cao. *$\mathcal{L}_1$ Adaptive Control Theory: Guaranteed Robustness with Fast Adaptation*, volume 21. SIAM, 2010.

[30] Randy Beard, Chengyu Cao, and Naira Hovakimyan. An $\mathcal{L}_1$ adaptive pitch controller for miniature air vehicles. In *AIAA Guidance, Navigation, and Control Conference and Exhibit*, page 6777, 2006. DOI: 10.2514/6.2006-6777.

[31] Elisa Capello, Giorgio Guglieri, Fulvia Quagliotti, and Daniele Sartori. Design and validation of an $\mathcal{L}_1$ adaptive controller for mini-UAV autopilot. *Journal of Intelligent & Robotic Systems*, 69(1-4):109–118, 2013.

[32] Isaac Kaminer, Antonio Pascoal, Enric Xargay, Naira Hovakimyan, Chengyu Cao, and Vladimir Dobrokhodov. Path following for small unmanned aerial vehicles using $\mathcal{L}_1$ adaptive augmentation of commercial autopilots. *Journal of Guidance, Control, and Dynamics*, 33(2):550–564, 2010. DOI: 10.2514/1.42056.

[33] Jiang Wang, Vijay Patel, Craig A. Woolsey, Naira Hovakimyan, and David Schmale. $\mathcal{L}_1$ adaptive control of a UAV for aerobiological sampling. In *American Control Conference (ACC'07)*, pages 4660–4665. IEEE, 2007.

[34] Yan Zhou, Huiying Liu, Huijuan Guo, and Xiaojun Duan. $\mathcal{L}_1$ adaptive dynamic inversion attitude control for unmanned aerial vehicle with actuator failures. *Proceedings of the Institution of Mechanical Engineers, Part G: Journal of Aerospace Engineering*, 233(11):4129–4140, 2019.

[35] Toufik Souanef. Multiple model $\mathcal{L}_1$ adaptive fault-tolerant control of small unmanned aerial vehicles. *Journal of Aerospace Engineering*, 2023. DOI: 10.1109/TIE.2016.2632682.

[36] Toufik Souanef. $\mathcal{L}_1$ adaptive output feedback control of small unmanned aerial vehicles. *Unmanned Systems*, 11(03):249–260, 2023. DOI: 10.1142/S2301385023500103.

[37] Toufik Souanef. *Adaptive Guidance and Control of Small Unmanned Aerial Vehicles*. Shaker Verlag, Germany, 2019.

[38] Enric Xargay, Vladimir Dobrokhodov, Isaac Kaminer, António M Pascoal, Naira Hovakimyan, and Chengyu Cao. Time-critical cooperative control of multiple autonomous vehicles. *IEEE Control Systems Magazine*, 32(5):49, 2012.

[39] G. Kumaresan and Alexander Kale. Application of $\mathcal{L}_1$ adaptive controller for the design of a novel decentralized leader follower formation algorithm. *IFAC-PapersOnLine*, 49(1):706–711, 2016.

[40] P. B. Sujit and S. Saripalli. Unmanned aerial vehicle path following. *IEEE Control Systems Magazine*, 34(1):42–59, 2014.

[41] Eugene Lavretsky and Kevin A. Wise. Robust adaptive control. In *Robust and Adaptive Control*, pages 317–353. Springer, 2013.

[42] Toufik Souanef, Ahsene Boubakir, and Walter Fichter. $\mathcal{L}_1$ adaptive control of systems with disturbances of unknown bounds. In J. Bordeneuve-Guibé, A. Drouin, and C. Roos, editors, *Advances in Aerospace Guidance, Navigation and Control.*, page 151. Springer, 2015. DOI: 10.1007/978-3-319-17518-8_10.

[43] Vadim Ivanovich Utkin. *Sliding modes and their application in variable structure systems*. Mir Publishers, 1978. In Russian.